

Structural and bonding character of potassium-doped *p*-terphenyl superconductors

Guo-Hua Zhong,^{1,2} Xiao-Hui Wang,² Ren-Shu Wang,³ Jia-Xing Han,² Chao Zhang,⁴ Xiao-Jia Chen,^{3,*} and Hai-Qing Lin^{2,†}

¹Shenzhen Institutes of Advanced Technology, Chinese Academy of Sciences, Shenzhen 518055, China

²Beijing Computational Science Research Center, Beijing 100193, China

³Center for High Pressure Science and Technology Advanced Research, Shanghai 201203, China

⁴Department of Physics, Yantai University, Yantai, 264005, China

(Dated: July 30, 2018)

Recently, there is a series of reports by Wang *et al.* on the superconductivity in K-doped *p*-terphenyl ($K_xC_{18}H_{14}$) with the transition temperatures range from 7 to 123 Kelvin. Identifying the structural and bonding character is the key to understand the superconducting phases and the related properties. Therefore we carried out an extensive study on the crystal structures with different doping levels and investigate the thermodynamic stability, structural, electronic, and magnetic properties by the first-principles calculations. Our calculated structures capture most features of the experimentally observed X-ray diffraction patterns. The K doping concentration is constrained to within the range of 2 and 3. The obtained formation energy indicates that the system at $x = 2.5$ is more stable. The strong ionic bonding interaction is found in between K atoms and organic molecules. The charge transfer accounts for the metallic feature of the doped materials. For a small amount of charge transferred, the tilting force between the two successive benzenes drives the system to stabilize at the antiferromagnetic ground state, while the system exhibits non-magnetic behavior with increasing charge transfer. The multifermionity of band structures near the Fermi level indicates that the driving force for superconductivity is complicated.

PACS numbers: 71.20.-b, 74.25.Jb, 74.70.-b, 74.70.Kn

I. INTRODUCTION

Superconducting materials have been a hot research topic in physics and materials science due to their important application values in energy, information, quantum devices and other advanced technologies. Researchers have been devoted to the design and synthesis of new superconducting materials, the understanding of superconducting mechanism and the exploration of superconductors with higher transition temperature (T_c). In 2010, the superconductivity of $T_c \sim 18$ Kelvin was discovered in potassium (K) metal doped picene¹, which opens a new avenue in the quest for organic hydrocarbon superconductors. Subsequently, the superconductivity has also observed in alkali, alkaline-earth metals and rare-earth elements doped phenanthrene²⁻⁵, chrysene⁵, phenacene⁶, coronene⁷, phenacene⁶ and 1,2;8,9-dibenzopentacene⁸, respectively. Especially, using density functional theory and Eliashberg's theory of superconductivity, we have predicted K-doped benzene ($K_2C_6H_6$) to be superconductive with the T_c around 6.2 Kelvin, and proposed that all hydrocarbons should show T_c in a similar temperature range of $5 < T_c < 7$ Kelvin under conventional conditions⁹. The results greatly increase the understanding of the superconductivity of polycyclic aromatic hydrocarbons (PAHs).

So far the highest T_c reached is 33.1 Kelvin in PAH superconductors, which was obtained in K-doped 1,2;8,9-dibenzopentacene⁸. However, previous theoretical studies showed that PAH superconductors usually exhibit the antiferromagnetic (AFM) ground state¹⁰⁻¹³ and exist the strong electronic correlation effects¹³⁻¹⁸, indicating the

superconducting mechanism is complicated in aromatic hydrocarbons. Our theoretical predictions have argued that electronic correlations⁹ or pressure¹⁹ could enhance high T_c in aromatic hydrocarbons. Hence, organic based compounds are candidates of high temperature or room temperature superconductors, since the interaction of electrons with much higher excitation energy than the phonon energy can result in a substantially higher T_c in these low dimensional materials^{20,21}. Thus, the higher T_c can be expected in this kind of aromatic hydrocarbons.

Recently, *p*-terphenyl ($C_{18}H_{14}$), a hydrocarbon compound containing three benzene rings connected by C-C bonding, draws a lot of attention. Different from the feature of sharing armchair edge in PAHs such as phenanthrene, chrysene, picene, coronene and 1,2;8,9-dibenzopentacene, benzene rings are connected by the single C-C bond in the *p*-terphenyl molecule. Namely, *p*-terphenyl is a non-polycyclic aromatic hydrocarbon. With regard to the study of superconductivity of this system, Wang *et al.* claimed the superconductivity of 7.2 Kelvin in the synthesized $K_xC_{18}H_{14}$ ²². Later, Wang *et al.* claimed to observe a higher T_c of 43 Kelvin²³ and even 123 Kelvin²⁴ in the K-doped *p*-terphenyl. They also ruled out the possibilities of the formation of K-doped C_{60} and graphite as suggested previously²⁵. By using high resolution photoemission spectroscopy on potassium surface-doped *p*-terphenyl crystals, Li *et al.* presented the spectroscopic evidence for pairing gaps at the surfaces of these materials, with the gaps persisting to 60 K or above²⁶. Furthermore, Liu *et al.* observed the superconductivity like transition at about 125 Kelvin in their fabricated potassium doped *p*-terphenyl with the help of

magnetization measurements²⁷. These subsequent works greatly promote the study to superconductivity of the material. However, the doping level and superconducting phases with different T_c have not been determined yet, not to mention the desired pairing mechanism. So identifying the structures and chemical bonds is crucial to the understanding of the superconducting phases as well as superconductivity, which is the focus of the current study.

p-Terphenyl has twisting degrees of freedom around the long molecular axis, which will result in complicated situations when K atoms are doped into *p*-terphenyl crystal. It has been well known that crystalized *p*-terphenyl exhibits two phases with the variation of temperature of $P2_1/c$ symmetry at room temperature and $P\bar{1}$ symmetry below 193 Kelvin^{28,29}. In addition, the pressure also drives a transition from C_2 to D_{2h} symmetry around 1.3 GPa³⁰. In this work, we will investigate the K doping effects on structural, electronic, and magnetic properties in *p*-terphenyl at ambient pressure by the first-principles calculations. The obtained structures will be compared with experiments. The details for the structural and bonding features will be provided. These results are helpful for the determination of the doping level and thermodynamically stable phases as well as the understanding of the charge transfer process and mechanism in these newly discovered superconductors.

II. METHOD

To study the structural and electronic properties of $K_xC_{18}H_{14}$, we employed the Vienna *ab initio* simulation package (VASP)^{31,32} based on the projector augmented wave method. For the plane-wave basis-set expansion, an energy cutoff of 600 eV was adopted. The Monkhorst-Pack k -point grids are generated according to the specified k -point separation of 0.02 \AA^{-1} and the convergence thresholds are set as 10^{-6} eV in energy and 10^{-3} eV/Å in force. The generalized gradient form (GGA) of the exchange-correlation functional (Perdew-Burke-Ernzerh of 96, PBE) was adopted³³. And considering the non-local interaction, we has added the correction of van der Waals (vdW) in version of vdW-DF2 in this calculation³⁴. The necessity of vdW-DF2 functional has been confirmed by our previous studies^{35,36}.

III. RESULTS

A. Determining functional

Starting from the pristine $C_{18}H_{14}$, we firstly optimized the crystal lattice parameters of solid $C_{18}H_{14}$ with the $P2_1/c$ symmetry to test the feasibility of vdW-DF2 functional. The obtained crystal lattice parameters from vdW-DF2 functional are $a = 13.569 \text{ \AA}$, $b = 5.542 \text{ \AA}$, $c = 7.911 \text{ \AA}$ and the angle $\beta = 92.8^\circ$, respectively. Seen

TABLE I: The optimized crystal lattice constants a , b , c , the angle β between two axes and the volume V of pristine $C_{18}H_{14}$ comparing with the experimental values.

Method	a (Å)	b (Å)	c (Å)	β (°)	V (Å ³)
Expt. ^a	13.613	5.613	8.106	92	619
Expt. ^b	13.621	5.613	8.116	92.01	621.1
Expt. ^c	13.59	5.59	8.08	92.9	613.4
Expt. ^d	13.58	5.58	8.02	92.10	607.3
Expt. ^e	13.55	5.63	8.15	92.60	621.1
vdW-DF2	13.569	5.542	7.911	92.8	594.2
LDA	13.215	5.292	7.443	93.57	519.6
GGA	13.596	6.283	8.574	88.89	732.2

^aRef. 37.

^bRef. 38.

^cRef. 39.

^dRef. 40.

^eRef. 41.

from the crystal lattice parameters listed in Table I, the vdW-DF2 functional products the lattice constants are in good agreement with experimental ones, though the small distinguish exists among those reported experimental observations³⁷⁻⁴¹. The error is respectively controlled within 2.5% for the lattice constant and 4% for the volume. But GGA and local density approximation (LDA)⁴² functional respectively extremely overestimates and underestimates the lattice constants (unit volume). The result indicates that the non local interaction should not be ignored in this aromatic hydrocarbon. As shown in Fig. 1, the calculated XRD spectrum of solid $C_{18}H_{14}$ shown in Fig. 1 fits the experiment done by Wang *et al.*²². Additionally, the average value of carbon-carbon bond lengths within the rings is about 1.40 \AA and those between rings are about 1.49 \AA , which are also consistent with experimental values²⁹.

B. Structure of $K_xC_{18}H_{14}$

Within the framework of the vdW-DF2 functional, we simulated K-doped *p*-terphenyl, and firstly considered three possible concentrations of $x = 1, 2$ and 3 in $K_xC_{18}H_{14}$. The total energy calculation indicates that the doping results in the phase transition of crystal structure. Both $K_1C_{18}H_{14}$ and $K_2C_{18}H_{14}$ are stabilized at $P2_1$ symmetry instead of $P2_1/c$. But $K_3C_{18}H_{14}$ can exist in form of $P2_1/c$ symmetry. The crystal lattice parameters at three doping levels are summarized in Table II. We find that the variation of crystal lattice parameters is complicated after doping. The intercalation of K atoms leads to the obvious expansion in b direction and the big contraction in c direction in $K_1C_{18}H_{14}$ and $K_2C_{18}H_{14}$. $K_3C_{18}H_{14}$ is abnormal since it expands in a and c directions while contracts in the b direction. However, the doping makes the system volume increase. Figure 2 clearly shows the characteristics of $K_xC_{18}H_{14}$ viewed from different directions. For $K_1C_{18}H_{14}$, as shown

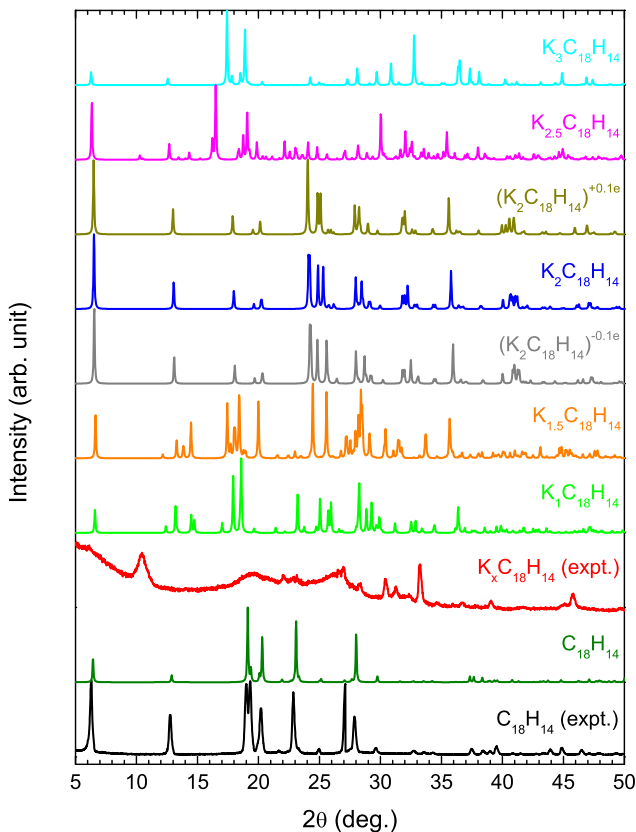


FIG. 1: (Color online) Calculated XRD spectra of pristine and K-doped $C_{18}H_{14}$ comparing with experiments²². The experimental XRD patterns of K-doped $C_{18}H_{14}$ were taken from the sample with $T_c = 7.2$ Kelvin. All XRD data was collected by using the incident wavelength $\lambda = 1.5406 \text{ \AA}$.

in Fig. 2(a), the herringbone structure is formed and K atom is between two organic molecular layers when viewing along the a direction, similar to K-doped picene¹ and phenanthrene². There is a tilted angle δ between two successive benzene rings with respect to each other, and it reaches the extent of $9.5^\circ - 10.6^\circ$. And viewing from the c direction, K atom is localized on the C-C bond connected benzene ring-1 with ring-2, and closer to ring-1. Scanning the fine bonding feature, we have found that the C-C bonds linked two benzene rings (hereafter call them as bridge bonds) are shortened to 1.46 \AA from 1.49 \AA while the C-C bonds near the bridge bond within the rings become long when one K atom is doped for every organic molecule. The variations of C-C bonds indicate that the charge is local near K atom instead of uniform distribution when transferring to π orbital from K atom.

For $K_2C_{18}H_{14}$, the herringbone structure is still existent as shown in Fig. 2(b). However, three benzene rings in organic molecule are almost coplanar. The tilted angle δ is only $0.2^\circ - 0.6^\circ$. Along the b direction, two K atoms are between two organic molecular layers, and viewing from the c direction, K atom respectively lies on the bridge bond. In $K_2C_{18}H_{14}$, the bridge bonds

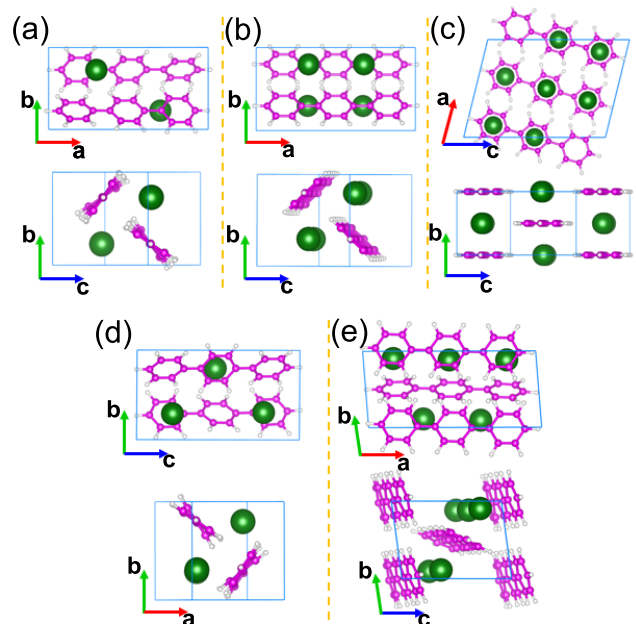


FIG. 2: (Color online) Optimized structures of $K_xC_{18}H_{14}$ viewing from different directions. Pink, white and green balls represent C, H and K atoms, respectively. (a) $K_1C_{18}H_{14}$, (b) $K_2C_{18}H_{14}$, (c) $K_3C_{18}H_{14}$, (d) $K_{1.5}C_{18}H_{14}$ and (e) $K_{2.5}C_{18}H_{14}$.

further shorten to 1.44 \AA and the C-C bonds near the bridge bond within the rings become longer. The distinguish of C-C bond lengths within the same ring becomes big which implies a stronger molecular distortion in $K_2C_{18}H_{14}$. Doping three K atoms into solid p -terphenyl, $K_3C_{18}H_{14}$, the system keeps the $P2_1/c$ symmetry, but great changes have taken place in the structure as shown in Fig. 2(c). All organic molecules rotate and form a visible two-dimensional layered structure. Along the b direction, three K atoms are all between two organic molecular layers, but viewing from the a direction, K atoms and p -terphenyl molecules are coplanar. Viewing from the b direction, the K atom is respectively on the center of benzene ring. The varying tendency of C-C bond lengths in $K_3C_{18}H_{14}$ is similar to $K_1C_{18}H_{14}$ and $K_2C_{18}H_{14}$. The bridge bonds further shorten to 1.43 \AA .

To identify the observed superconducting phase in experiment, we have analyzed the XRD result. Compared the experimental XRD between $C_{18}H_{14}$ and $K_xC_{18}H_{14}$ with 7.2 Kelvin superconductivity, the abnormal peaks around $2\theta = 10.4^\circ$ and $2\theta = 33.2^\circ$ imply the formation of new phase and a possible phase transition after doping. Additionally, the wide XRD peaks indicate that the crystallinity of the sample is not very good so that mixture phase can exist. Our calculated XRD of $K_1C_{18}H_{14}$, $K_2C_{18}H_{14}$ and $K_3C_{18}H_{14}$ are presented in Fig. 1. Unfortunately, we find that none of three structures is completely consistent with the experiment in XRD spectrum. Although the XRD of $K_2C_{18}H_{14}$ or $K_3C_{18}H_{14}$ is closer to the experimental result, the XRD

TABLE II: The optimized crystal lattice constants a , b , c , the angle β between two axes, the tilted angle δ between two successive benzene rings with respect to each other and the volume V for every doping level.

System	Space-group	a (Å)	b (Å)	c (Å)	α (°)	β (°)	γ (°)	δ (°)	V (Å ³)
K ₁ C ₁₈ H ₁₄	$P2_1$	13.500	6.863	7.181	90	83.12	90	9.5-10.6	660.6
K _{1.5} C ₁₈ H ₁₄	$P1$	7.110	7.274	14.743	89.76	64.56	90.02	17.2-20.3	688.6
K ₂ C ₁₈ H ₁₄	$P2_1$	14.001	7.032	7.151	90	75.54	90	0.2-0.6	681.8
K _{2.5} C ₁₈ H ₁₄	$P1$	14.585	6.278	9.058	99.25	73.54	96.77	1.1-2.5	782.7
K ₃ C ₁₈ H ₁₄	$P2_1/c$	14.503	5.463	10.243	90	76.13	90	0	787.8

peak around $2\theta = 10.4^\circ$ has not observed in these two pure phases. Thus we further investigated the possibility of other doped phases. On the one hand, we added a small charge fluctuation into K₂C₁₈H₁₄ to form defect state, such as (K₂C₁₈H₁₄)^{+0.1e} and (K₂C₁₈H₁₄)^{-0.1e}. However, except for the small shift of peaks, this did not change the XRD spectrum in nature as shown in Fig. 1. On the other hand, we considered the fractional doping concentrations, such as K_{1.5}C₁₈H₁₄ or K_{2.5}C₁₈H₁₄, which can also understood as a mixed phase. In experiment, K_{1.5}C₁₈H₁₄ may be obtained by mixing K₁C₁₈H₁₄ and K₂C₁₈H₁₄, while K_{2.5}C₁₈H₁₄ can be formed by mixing K₂C₁₈H₁₄ and K₃C₁₈H₁₄. By subtracting and adding K atoms from/into K₂C₁₈H₁₄, we have simply simulated the fractional doping levels in this calculation. Table II and Figure 2 present the optimized crystal lattice parameters and geometrical configurations, respectively. Both K_{1.5}C₁₈H₁₄ and K_{2.5}C₁₈H₁₄ are stabilized at $P1$ symmetry. The volumes of unit cell of doping cases of $x = 1, 1.5, 2, 2.5$ and 3 does not satisfy the monotonically increasing trend due to the existence of phase transitions during the doping. As shown in Fig. 2(d), K_{1.5}C₁₈H₁₄ is similar to K₁C₁₈H₁₄. There are a visible herringbone feature and a big tilted angle between two successive benzene rings with respect to each other. The asymmetric distribution of K atoms in K_{2.5}C₁₈H₁₄ (Fig. 2(e)) did not cause the big rotation between two successive benzene rings with respect to each other. However, the arrangement of organic molecules appears more arbitrary in K_{2.5}C₁₈H₁₄. Comparing their XRD with the experiment one in Fig. 1, we were surprised to find that K_{2.5}C₁₈H₁₄ produced some peaks fitting experiment near $2\theta = 10.4^\circ$ and $2\theta = 33.2^\circ$ and being not observed in K_{1.5}C₁₈H₁₄. Of course, the XRD obtained from K_{2.5}C₁₈H₁₄ can not completely match that of experiment, either. Seen from the XRD result, the superconducting phase observed in the experiment is more like a mixed phase by K₂C₁₈H₁₄ and K₃C₁₈H₁₄.

C. Stability

To examine the thermodynamic stability of these considered doping cases, we have calculated the formation energy E_f . The E_f for the doping level x is defined as the function of K chemical potential the following as

$$E_f = E_{\text{doped}} - E_{\text{pristine}} - x\mu_{\text{K}}^{\text{bulk}} - x[\mu_{\text{K}} - \mu_{\text{K}}^{\text{bulk}}] \quad (1)$$

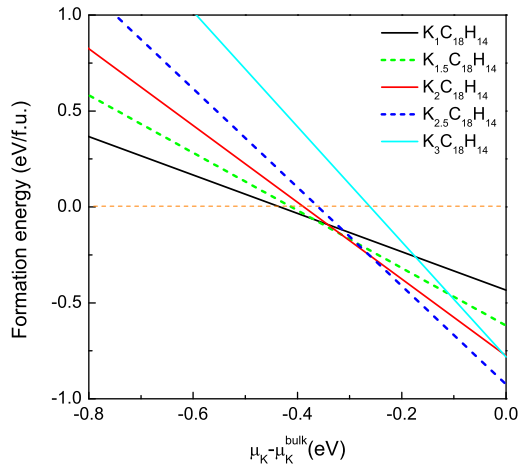


FIG. 3: (Color online) Calculated formation energy of $K_x C_{18} H_{14}$ as a function of the K chemical potential.

where E_{doped} and E_{pristine} is the total energy of the doped and host crystal, respectively. $\mu_{\text{K}}^{\text{bulk}}$ can be obtained from the energy per K atom in the K metal with the bcc structure. x is the doping concentration. μ_{K} is the chemical potential of the K specie. $\mu_{\text{K}} = \mu_{\text{K}}^{\text{bulk}}$ means the element is so rich that the pure element phase can form. $E_f < 0$ indicates that the doped compound can stably exist. From the calculated formation energy shown in Fig. 3, all of considered doped phases are able to exist as the chemical potential of K satisfying certain conditions. Comparing several doping levels, however, K_{2.5}C₁₈H₁₄ is more stable since it has the lower formation energy than other phases in a wide range of chemical potential. This suggests that the experimentally observed superconducting phase of 7.2 K shall be K_{2.5}C₁₈H₁₄ or a mixture phase.

D. Bonding character and charger transfer

Similar to other PAH superconductors, K-doped p-Terphenyl possesses the typical feature of charge transfer salt. Analyzing the interaction between K atoms and organic molecules, we can observe the clear ionic bonding characteristic. The different charge density $\Delta\rho$ [$\Delta\rho = \rho(K_x C_{18} H_{14}) - \rho(C_{18} H_{14}) - \rho(K_x)$] shown in Fig. 4 graphically depicts the charge transferring between K

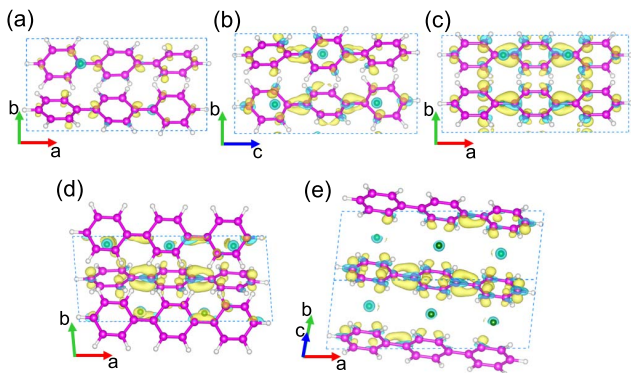


FIG. 4: (Color online) Calculated 3D plots of different charge density for $K_x C_{18} H_{14}$ with the iso-surface unit of $5 \times 10^{-3} e/a.u.^3$. Pink, white and green balls represent C, H and K atoms, respectively. The yellow and light blue areas mean the increase and the decrease of electrons in this region, respectively. (a) $K_1 C_{18} H_{14}$, (b) $K_{1.5} C_{18} H_{14}$, (c) $K_2 C_{18} H_{14}$, (d) $K_{2.5} C_{18} H_{14}$ and (e) $K_3 C_{18} H_{14}$.

atoms and organic molecules. The yellow and light blue areas define as the gain and loss of electrons, respectively. With the increase of doping content, the quantity of transferred charge is about 0.84, 1.24, 1.65, 1.99 and 2.44 e/f.u. for $K_1 C_{18} H_{14}$, $K_{1.5} C_{18} H_{14}$, $K_2 C_{18} H_{14}$, $K_{2.5} C_{18} H_{14}$ and $K_3 C_{18} H_{14}$, respectively. As mentioned above, the superconducting phase observed by experiment is predicted as a mixed phase such as the doping level around $x \sim 2.5$. Then the transferring charge of about two electrons is suggested. Another important information from $\Delta\rho$ is that it visibly shows the distribution of charge transferred to C atoms. As shown in Fig. 4, the transferred charge distribution is neither local nor homogeneous. The charge is distributed on part C atoms in certain an symmetrical ordering and highlights the distribution near bridge bonds. As a comparison, the added charge mainly concentrates on the middle benzene ring with the increase of K content. To $K_3 C_{18} H_{14}$, the distribution of transferred charge covers all C atoms.

E. Electronic structures

The pristine *p*-terphenyl is a wide-gap semiconductor with the bandgap of 3.3 eV⁴³. The charge transferring from K atoms to organic molecules makes Fermi level shift toward to higher energy, which results in a transition from insulator to metal. Figure 5 and 6 respectively show the band structure and the total density of states (DOS) for each doping level at non-magnetic (NM) state. Under $P2_1$ symmetry, the conjugated molecules splits each orbital into a pair of partly degenerate bands in $K_1 C_{18} H_{14}$. As shown in Fig. 5(a), two partly degenerate bands forming the first group conduction band cross Fermi level. However, transforming to $K_{1.5} C_{18} H_{14}$ with $P1$ symmetry (Fig. 5(b)), the coupling between

the two conjugated molecules is weakened, which leads to a bigger splitting of bands. These former two doping levels both drive the high DOS at Fermi level (N_{EF}) as shown in Fig. 6(a) and 6(b). The values of N_{EF} are 10.25 and 10.43 states/eV/f.u. for $K_1 C_{18} H_{14}$ and $K_{1.5} C_{18} H_{14}$, respectively. More electrons transferring to organic molecules, in $K_2 C_{18} H_{14}$ shown in Fig. 5(c), the Fermi level moves into the overlap region of two group of conduction bands formed by two molecular orbitals. $K_2 C_{18} H_{14}$ exhibits the weak metallic feature with a small N_{EF} value of 1.28 states/eV./f.u. as shown in Fig. 6(c). In $K_{2.5} C_{18} H_{14}$ (Fig. 5(d)), more electrons transferring to organic molecules rises Fermi level into the second group of conduction band. However, the conjugated character of organic molecules completely disappears, which further weakens the coupling among bands. One band crosses Fermi level, differing from the two-band model in other doping cases. The Fermi level is localized at a DOS peak (Fig. 6(d)) which results in a slightly big N_{EF} value of 5.1 states/eV/f.u.. For $K_3 C_{18} H_{14}$ with $P2_1/c$ symmetry, as shown in Fig. 5(e), the Fermi level moves into the second group of conduction band. The interactions between K atoms and molecules strengthen which makes bands become more extended. As shown in Fig. 6(e), a stronger metallic feature (3.57 states/eV/f.u. for N_{EF}) is observed in $K_3 C_{18} H_{14}$ than $K_2 C_{18} H_{14}$. The result of electronic structures also indicates that we can obtain higher N_{EF} value by tuning the chemical potential of K to realize the high superconductivity, which is consistent with Mazziotti's suggestion⁴⁴.

Previous studies have pointed out that doped PAHs are often at the AFM ground state^{10–13}. Hence, we have investigated the magnetism of K-doped *p*-terphenyl. It was found that both $K_1 C_{18} H_{14}$ and $K_{1.5} C_{18} H_{14}$ are at the AFM ground state. The total energy of AFM state is respectively 40.4 meV for $K_1 C_{18} H_{14}$ and 9.2 meV for $K_{1.5} C_{18} H_{14}$ less than that of their NM state. The local magnetic moment are respectively 0.57 and 0.22 μ_B /f.u. for $K_1 C_{18} H_{14}$ and $K_{1.5} C_{18} H_{14}$, respectively. The electronic states at Fermi level shown in Fig. 7 visibly decrease, and the values of N_{EF} reduce to 1.6 and 5.5 states/eV/f.u. for $K_1 C_{18} H_{14}$ and $K_{1.5} C_{18} H_{14}$, respectively. Interestingly, all of $K_2 C_{18} H_{14}$, $K_{2.5} C_{18} H_{14}$ and $K_3 C_{18} H_{14}$ are stabilized at NM state. Comparing these magnetic structures in K-doped *p*-terphenyl, the difference of magnetism possibly results from the distortion in organic molecular plane. As shown in Fig. 2, the tilt between two successive benzene rings drives the spin ordering of electrons transferred to C atoms from K atoms. With the increase of charge transferring, the spin ordering disappears in systems while the superconductivity occurs.

F. Discussions

With regard to the superconductivity of K-doped *p*-terphenyl, more data and analysis are yet to come. The

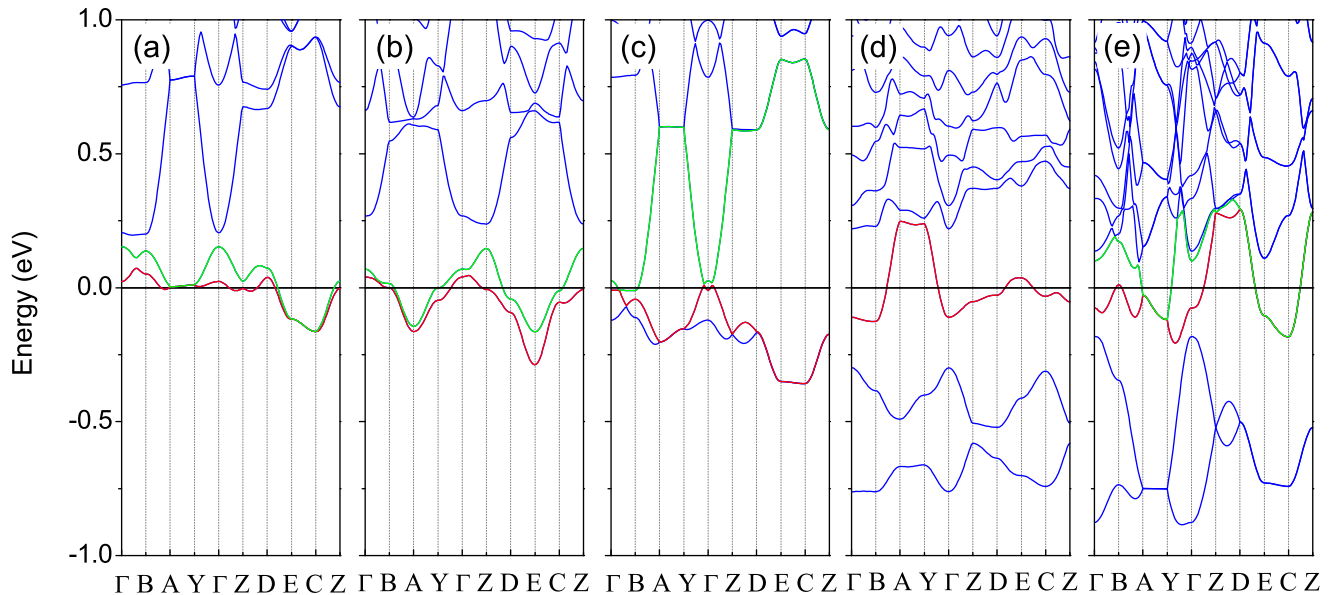


FIG. 5: (Color online) Electronic band structures of $K_x C_{18} H_{14}$ at NM state. Zero energy denotes the Fermi level. (a) $K_1 C_{18} H_{14}$, (b) $K_{1.5} C_{18} H_{14}$, (c) $K_2 C_{18} H_{14}$, (d) $K_{2.5} C_{18} H_{14}$ and (e) $K_3 C_{18} H_{14}$.

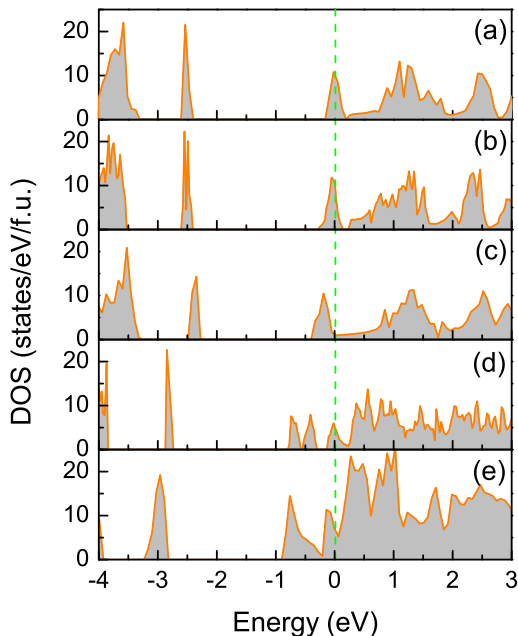


FIG. 6: (Color online) Electronic DOS of $K_x C_{18} H_{14}$ at NM state. Zero energy denotes the Fermi level. (a) $K_1 C_{18} H_{14}$, (b) $K_{1.5} C_{18} H_{14}$, (c) $K_2 C_{18} H_{14}$, (d) $K_{2.5} C_{18} H_{14}$ and (e) $K_3 C_{18} H_{14}$.

complexity of superconducting mechanism in K-doped *p*-terphenyl is evidenced by recent reported three critical temperatures, 7.2, 43 and 123 Kelvin, in the same material^{22–24}. In previous studies, however, we have pointed out that there is a common phase to show T_c

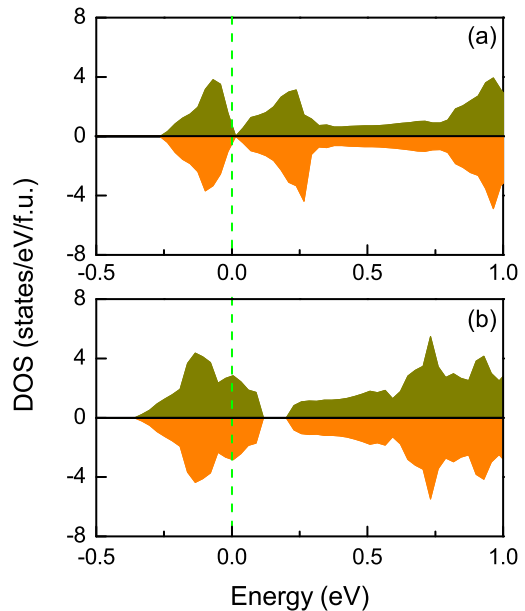


FIG. 7: (Color online) Electronic DOS of $K_1 C_{18} H_{14}$ (a) and $K_{1.5} C_{18} H_{14}$ (b) with the AFM spin polarization. Zero energy denotes the Fermi level.

in the range of $5 < T_c < 7$ Kelvin in all K-doped aromatic compounds⁹. The existed superconductivity of 7.2 Kelvin in K-doped *p*-terphenyl just confirms that prediction. For this low T_c phase, the electron-phonon coupling mechanism is enough to describe this superconductivity. From previous investigations^{9,45}, the phonons with low and middle frequency mainly contribute to electron-

phonon interaction. The maximum value of our calculated the middle frequency of $\text{K}_2\text{C}_{18}\text{H}_{14}$ is about 1574 cm^{-1} which is almost equal to that of K-doped picene⁴⁵ and also comparable with that of $\text{K}_2\text{C}_6\text{H}_6$ ⁹. At the same time, the N_{E_F} can change with the doping content around 5.1 states/eV/f.u. for $\text{K}_{2+\delta}\text{C}_{18}\text{H}_{14}$ ($0 < \delta < 1$) due to the charge fluctuations. Based on the comparable N_{E_F} of K-doped *p*-terphenyl with K-doped benzene and picene in the range of 4 – 6 states/eV/f.u.^{9,45}, and combining with the similar feasible screened Coulomb pseudopotential μ^* of 0.1, we can predict that the T_c of K-doped *p*-terphenyl is in the range of $5 < T_c < 7$ Kelvin, which is according with the experimental observation²³. In other words, the observed superconducting phase is a mixed compound in the doping range of $2 < x < 3$ instead of pure $\text{K}_1\text{C}_{18}\text{H}_{14}$ or $\text{K}_{1.5}\text{C}_{18}\text{H}_{14}$ phase, which is just what we predicted by XRD, thermodynamic stability, electronic and magnetic properties.

With regarded to higher transition temperature, the experimental investigations presented unknown peaks in Raman spectra. These unknown peaks are possibly induced by graphite, C_{60} and other modes^{23,24}. On the one hand, therefore, we infer that the two higher transition temperatures may be from other new superconducting modes such as CK_x , KH_x and K-CH_x compounds induced by the reconstruction. On the other hand, as our previous studies^{9,19}, some internal and external factors can be the cause of high superconducting transition temperature, such as electronic correlations and pressure. The strong electronic correlations in K-doped *p*-terphenyl were implied by Baskaran⁴⁶ and Fabrizio *et al.*⁴⁷. In this kind of low dimensional organic system, therefore, the high superconductivity may be related with the electronic correlations effects. To clarify the matter, more efforts in the future are surely needed.

IV. CONCLUSIONS

In conclusion, with the aim of exploring the structural and bonding characteristics of K-doped *p*-terphenyl which has been discovered to be a superconductor with

$T_c = 7.2 - 123$ Kelvin, we have carried out the first-principles calculations based on vdW-DF2 functional. Considering five doping levels of $x = 1, 1.5, 2, 2.5$ and 3 in $\text{K}_x\text{C}_{18}\text{H}_{14}$, we have predicted the optimized crystal structures at each doping level, calculated the XRD spectra, and investigated the thermodynamic stability, ionic bonding characteristics, charge transfer, electronic and magnetic properties. All of these five doping phases are able to exist in experiment based on the negative formation energy, but $\text{K}_{2.5}\text{C}_{18}\text{H}_{14}$ or say a mixed phase by $\text{K}_2\text{C}_{18}\text{H}_{14}$ and $\text{K}_3\text{C}_{18}\text{H}_{14}$ is more stable in a wide range of chemical potential. The XRD summarized by $\text{K}_2\text{C}_{18}\text{H}_{14}$, $\text{K}_{2.5}\text{C}_{18}\text{H}_{14}$ and $\text{K}_3\text{C}_{18}\text{H}_{14}$ can almost match that of experiment. The charge transfer from K atoms to organic molecules results in the insulator-metal transition. However, both $\text{K}_1\text{C}_{18}\text{H}_{14}$ and $\text{K}_{1.5}\text{C}_{18}\text{H}_{14}$ are stabilized at AFM ground state, while the latter three compounds exhibit the non-magnetic behavior. The superconducting phase observed in experiment should be a mixture phase with doping level in range of $2 < x < 3$. However, the multifermionity of band structures near Fermi level indicates that the driving force for superconductivity is complicated. Future works are needed to understand the superconductivity especial for the transition temperature above 40 Kelvin.

V. ACKNOWLEDGMENTS

The work was supported by the National Natural Science Foundation of China (Grant Nos. 61574157 and 61774164) and the Basic Research Program of Shenzhen (Grant nos. JCYJ20160331193059332, JCYJ20150529143500956 and JCYJ20150401145529035). H. Q. Lin, X. H. Wang, J. X. Han and G. H. Zhong acknowledge support from NSAF U1530401 and computational resource from the Beijing Computational Science Research Center. The partial calculation was supported by the Special Program for Applied Research on Super Computation of the NSFC-Guangdong Joint Fund (the second phase) under Grant No. U1501501.

* Electronic address: xjchen@hpstar.ac.cn

† Electronic address: haiqing0@csrc.ac.cn

¹ R. Mitsuhashi, Y. Suzuki, Y. Yamanari, H. Mitamura, T. Kambe, N. Ikeda, H. Okamoto, A. Fujiwara, M. Yamaji, N. Kawasaki, Y. Maniwa, and Y. Kubozono, *Nature (London)* **464**, 76 (2010).

² X. F. Wang, R. H. Liu, Z. Gui, Y. L. Xie, Y. J. Yan, J. J. Ying, X. G. Luo, and X. H. Chen, *Nat. Commun.* **2**, 507 (2011).

³ X. F. Wang, Y. J. Yan, Z. Gui, R. H. Liu, J. J. Ying, X. G. Luo, and X. H. Chen, *Phys. Rev. B* **84**, 214523 (2011).

⁴ X. F. Wang, X. G. Luo, J. J. Ying, Z. J. Xiang, S. L. Zhang, R. R. Zhang, Y. H. Zhang, Y. J. Yan, A. F. Wang,

P. Cheng, G. J. Ye, and X. H. Chen, *J. Phys.: Condens. Matter* **24**, 345701 (2012).

⁵ G. A. Artioli, F. Hammerath, M. C. Mozzati, P. Carretta, F. Corana, B. Mannucci, S. Margadonna, and L. Malavasi, *Chem. Commun.* **51**, 1092 (2015).

⁶ Y. Kubozono, H. Goto, T. Jabuchi, T. Yokoya, T. Kambe, Y. Sakai, M. Izumi, L. Zheng, S. Hamao, H. L. T. Nguyen, M. Sakata, T. Kagayama, and K. Shimizu, *Physica C* **514**, 199 (2015).

⁷ Y. Kubozono, M. Mitamura, X. Lee, X. He, Y. Yamanari, Y. Takahashi, Y. Suzuki, Y. Kaji, R. Eguchi, K. Akaike, T. Kambe, H. Okamoto, A. Fujiwara, T. Kato, T. Kosugi, and H. Aoki, *Phys. Chem. Chem. Phys.* **13**, 16476 (2011).

- ⁸ M. Q. Xue, T. B. Cao, D. M. Wang, Y. Wu, H. X. Yang, X. L. Dong, J. B. He, F. W. Li, and G. F. Chen, *Sci. Rep.* **2**, 389 (2012).
- ⁹ G. Zhong, X.-J. Chen, and H.-Q. Lin, e-print arXiv:1501.00240 (to be published).
- ¹⁰ G.-H. Zhong, C. Zhang, G.-F. Wu, Z.-B. Huang, X.-J. Chen, and H.-Q. Lin, *J. Appl. Phys.* **113**, 17E131 (2013).
- ¹¹ G. Zhong, Z. Huang, and H. Lin, *IEEE T. Magn.* **50**, 1700103 (2014).
- ¹² X.-W. Yan, Y. Wang, M. Gao, D. Ma, and Z. Huang, *J. Phys. Chem. C* **120**, 22565 (2016).
- ¹³ G. Giovannetti and M. Capone, *Phys. Rev. B* **83**, 134508 (2011).
- ¹⁴ M. Kim, B. I. Min, G. Lee, H. J. Kwon, Y. M. Rhee, and J. H. Shim, *Phys. Rev. B* **83**, 214510 (2011).
- ¹⁵ Z. Huang, C. Zhang, and H.-Q. Lin, *Sci. Rep.* **2**, 922 (2012).
- ¹⁶ A. Ruff, M. Sing, R. Claessen, H. Lee, M. Tomić, H. O. Jeschke, and R. Valentí, *Phys. Rev. Lett.* **110**, 216403 (2013).
- ¹⁷ J.-X. Han, G.-H. Zhong, X.-H. Wang, X.-J. Chen, and H.-Q. Lin, *AIP Adv.* **7**, 055704 (2017).
- ¹⁸ X.-H. Wang, G.-H. Zhong, J.-X. Han, X.-J. Chen, and H.-Q. Lin, *AIP Adv.* **7**, 055707 (2017).
- ¹⁹ G.-H. Zhong, C.-L. Yang, X.-J. Chen, and H.-Q. Lin, e-print arXiv:1612.01217 (to be published).
- ²⁰ W. A. Little, *Phys. Rev.* **134**, A1416 (1964).
- ²¹ V. L. Ginzburg, *Sov. Phys. Usp.* **19**, 174 (1976).
- ²² R.-S. Wang, Y. Gao, Z.-B. Huang, and X.-J. Chen, e-print arXiv:1703.05803 (to be published).
- ²³ R.-S. Wang, Y. Gao, Z.-B. Huang, and X.-J. Chen, e-print arXiv:1703.05804 (to be published).
- ²⁴ R.-S. Wang, Y. Gao, Z.-B. Huang, and X.-J. Chen, e-print arXiv:1703.06641 (to be published).
- ²⁵ Y. Gao, R.-S. Wang, X.-L. Wu, J. Cheng, T.-G. Deng, X.-W. Yan, and Z.-B. Huang, *Acta Phys. Sin.* **65**, 077402 (2016).
- ²⁶ H. Li, X. Zhou, S. Parham, T. Nummy, J. Griffith, K. Gordon, E. L. Chronister, and D. S. Dessau, e-print arXiv:1704.04230 (to be published).
- ²⁷ W. Liu, H. Lin, R. Kang, X. Zhu, Y. Zhang, S. Zheng, and H.-H. Wen, *Phys. Rev. B* **96**, 224501 (2017).
- ²⁸ J. L. Baudour, Y. Delugeard, H. Cailleau, *Acta Cryst.* **B32**, 150 (1976).
- ²⁹ J. L. Baudour, H. Cailleau, W. B. Yelon, *Acta Cryst.* **B33**, 1773 (1977).
- ³⁰ T. Liu, S. Xu, C. Sun and M. Zhou, *Chem. Phys. Lett.* **615**, 1 (2014).
- ³¹ G. Kresse and J. Furthmuller, *Comput. Mater. Sci.* **6**, 15 (1996).
- ³² G. Kresse and J. Furthmuller, *Phys. Rev. B* **54**, 11169 (1996).
- ³³ J. P. Perdew, K. Burke, M. Ernzerhof, *Phys. Rev. Lett.* **77**, 3865 (1996).
- ³⁴ K. Lee, É. D. Murray, L. Kong, B. I. Lundqvist, D. C. Langreth, *Phys. Rev. B* **82**, 081101(R) (2010).
- ³⁵ G.-H. Zhong, C. Zhang, X. Yan, X. Li, Z. Du, G. Jing, and C. Ma, *Mol. Phys.* **115**, 472 (2017).
- ³⁶ X. Wang, G. Zhong, X. Yan, X. Chen, and H. Lin, *J. Phys. Chem. Solids* **104**, 56 (2017).
- ³⁷ H. M. Rietveld, E. N. Maslen, C. T. B. Clews, *Acta Cryst.* **B26**, 693 (1970).
- ³⁸ H. Saitoh, K. Saito, Y. Yamamura, H. Matsuyama, K. Kikuchi, M. Lyoda, I. Ikemoto, *Bull. Chem. Soc. Jpn.* **66**, 2847 (1993).
- ³⁹ P. Puschnig, G. Heimel, K. Weinmeier, R. Resel, and C. Ambrosch-Draxl, *High Pressure Res.* **22**, 105 (2002).
- ⁴⁰ N. A. Murugan and S. Yashonath, *J. Phys. Chem. B* **109**, 1433 (2005).
- ⁴¹ S. Selvakumar, K. Sivaji, N. Balamurugan, A. Arulchakkaravarthi, S. Sankar, C. Venkateswaran, and P. Ramasamy, *J. Cryst. Growth* **275**, e265 (2005).
- ⁴² D. M. Ceperley and B. J. Alder, *Phys. Rev. Lett.* **45**, 566 (1980).
- ⁴³ K. Yoshino, M. Hirohata, K. Tada, A. Fujii, M. Ozaki, A. Naka, and M. Ishikawa, *Proc. SPIE* **3145**, 192 (1997).
- ⁴⁴ M. V. Mazziotti, A. Valletta, G. Campi, D. Innocenti, A. Perali, and A. Bianconi, *EPL* **118**, 37003 (2017).
- ⁴⁵ M. Casula, M. Calandra, G. Profeta, and F. Mauri, *Phys. Rev. Lett.* **107**, 137006 (2011).
- ⁴⁶ G. Baskaran, e-print arXiv:1704.08153 (to be published).
- ⁴⁷ M. Fabrizio, T. Qin, S. S. Naghavi, and E. Tosatti, e-print arXiv:1705.05066 (to be published).